e-ISSN 2320 –7876 www.ijfans.org
Vol.11, Iss.9, Dec 2022

Research Paper

SIMPLE COMBUSTION SYNTHESIS AND PHYSICAL CHARACTERIZATION STUDIES OF NI-ZNS NANOPARTICLES

K. Ganesh[1,*], G. Padma Priya[1]
[1] Department of Chemistry, Faculty of Arts and Science,
Bharath Institute of Higher Education and Research (BIHER),
Chennai – 600073, Tamil Nadu, India
***Corresponding Author Email addresses: ganmass7986@gmail.com** (K. Ganesh)

Address for Correspondence

K. Ganesh[1,*], G. Padma Priya[1]
[1] Department of Chemistry, Faculty of Arts and Science,
Bharath Institute of Higher Education and Research (BIHER),
Chennai – 600073, Tamil Nadu, India
***Corresponding Author Email addresses: ganmass7986@gmail.com** (K. Ganesh)

Abstract

In this paper, nanostructured Ni-ZnS nanocatalysts were synthesized through a facile microwave combustion route. Powder XRD, FT-IR, EDX and SAED patterns revealed the presence of material in well crystalline single phase with average crystallite size of about 15 nm and the material remained cubic over the whole Ni-ZnS. Formation of ultrafine, spherical and homogeneous dispersed NPs with size 20 nm was confirmed by SEM and TEM analysis. VSM results confirmed a weak superparamagnetic behavior of Ni-ZnS and the values of M_s gradually increased with increasing the concentration of Ni^{2+} cations. The room temperature PL spectra of Ni-ZnS NPs showed extra peaks in yellow–orange and red region in comparison of undoped ZnS NPs. PL spectra was suggested with the significant enhancement of the PL intensity in Ni-ZnS NPs, due to Ni^{2+} incorporation.

Keywords: Ni-ZnS; Microwave combustion; Magnetic properties; Optical properties.

1. Introduction

Nowadays, metal sulfide nanomaterials are also of interest, due to their unique applications as, amongst others, semiconductors, solar radiation absorbers, catalysts, polymer

surface coatings, electro luminescent devices and multilayer dielectric filters [1-5]. Among them, zinc sulfide, ZnS have many applications as a result of their metal- like electrical conductivity, chemical sensing capabilities, photo-catalysts [6-8]. Usually, metal sulfides allow the introduction of different metal ions, which can changes their physico-chemical properties considerably. Doped semiconductors are being studied intensively to achieve three different material properties, viz. luminescence, magnetic and catalytic properties [9-12]. If the impurity atoms have unfilled '*d*' electrons, then one also observes the magnetic properties [13]. Ni-ZnS NPs have been mainly studied due to their luminescence properties [14]. The excited electrons are transferred from the conduction band, which the radiative de-excitation occurs via $^4T_1$-$^6A_1$ transitions. The optical and magnetic properties have been studied in a few doped nanomaterials [15-20].

Several methods have been used to prepare metal sulfide nanomaterials, such as hydrothermal, solvothermal, ball-milling, microemulsion, thermal decomposition methods, etc. However, the above methods have some disadvantageous such as complicated equipment and costly chemicals (surfactants or templates), higher temperature, need longer reaction time and higher pressure. Also, from the viewpoint of green chemistry, the use of surfactants or templates is main disadvantageous, due to unavoidably increase the reaction complexity, results in impurity products [21-25].

Therefore, the development of simple, efficient and surfactant- free methods for the controlled synthesis of functional nanomaterials is highly desirable. In our case, Ni-ZnS nano-photocatalysts could be prepared within 10 min at low temperature by MCM. However, this MCM approach is interesting route and proved as a one-step to produce such advanced nanomaterials, because of energy consuming, convenient, economical and environmentally friendly, low cost, high efficiency, low temperature and also potential for nano-scale products.

2. Experimental part

Materials and methods

The reagents of zinc nitrate ($Zn(NO_3)_2.6H_2O$), nickel nitrate ($Ni(NO_3)_2{\cdot}4H_2O$), and thiourea ($CS(NH_2)_2$) used were of analar grade obtained from Merck, India and were used as received without further purification. The samples were prepared with the addition of Mn^{2+} of different molar ratios (Ni-ZnS) to ZnS. Stoichiometric amounts of $Zn(NO_3)_2.6H_2O$,

$Ni(NO_3)_2 \cdot 4H_2O$ and $CS(NH_2)_2$ were dissolved in deionized water and poured into a silica crucible, which was placed in a domestic microwave-oven and exposed to the microwave energy in a 2.45 GHz multimode cavity at 900 W for 10 minutes. The raw materials decompose and yield flammable gases such as H_2O, N_2, NO, and CO_2, respectively. Primarily, the raw materials boiled and underwent evaporation followed by the decomposition with the evolution of gases. After the precursor solution reaches the point of spontaneous combustion, it begins burning and instantly becomes a solid and then used for further characterizations.

2.2. Characterization techniques

The structural characterization of Ni-ZnS nano-crystals were performed using a Philips PAN analytical X' pert PRO diffractometer equipped with a Cu tube for generating a Cu Kα radiation (wavelength 1.5406 Å) at 40 kV, 25 mA. The surface functional groups were analyzed by Thermo Nickolet FT-IR spectrometer. The samples were incorporated in KBr pellets for the measurements. Morphological studies and energy dispersive X-ray (EDX) analysis have been performed with a Jeol JSM6360 high resolution scanning electron microscopy (HR-SEM). The transmission electron micrographs (TEM) were carried out by Philips-TEM (CM20). The surface area was derived from the N_2 adsorption-desorption isotherms using liquid nitrogen at 77 K using an automatic adsorption instrument (Quantachrome Corp. Nova-1000 gas sorption analyzer). The UV-Visible diffuse reflectance spectrum (DRS) was recorded using Varian Cary 5E UV/VIS-NIR UV-Visible spectrophotometer to estimate their band gap energy (E_g). The photoluminescence (PL) properties were recorded at room temperature using Perkin Elmer LS 55 Fluorescence Spectrophotometer. VSM measurements were performed by using a Vibrating sample magnetometer (LDJ Electronics Inc., Model 9600). The magnetization measurements were carried out in an external field upto 10 kOe at room temperature.

3. Results and discussion

Powder XRD analysis

Fig. 1 shows the powder XRD patterns of Ni-ZnS NPs and the observed diffraction peaks are assigned to (111), (220) and (311) planes of the zinc blende (cubic) phase of ZnS which are in good agreement with the literature values of JCPDS card no. 5-0568 [26]. The results indicate that ZnS NPs are crystalline, pure and ordered at long range. The average crystallite size of single phase Ni-ZnS were calculated by using Debye Scherrer formula in Eq. (1):

e-ISSN 2320 –7876 www.ijfans.org
Research Paper
Vol.11, Iss.9, Dec 2022

$$L = \frac{0.89\lambda}{\beta \cos\theta} \quad \text{------ (1)}$$

where *'L'* is the average crystallite size, *'λ'*, the X-ray wavelength (1.5406 Å), *'β'*, full width at half maximum (FWHM) and *'θ'*, the Bragg angle of the planes. It has been observed that the average crystallite size is decreased from 17.65 to 15.25 nm with increase the Ni^{2+}-dopant [27].

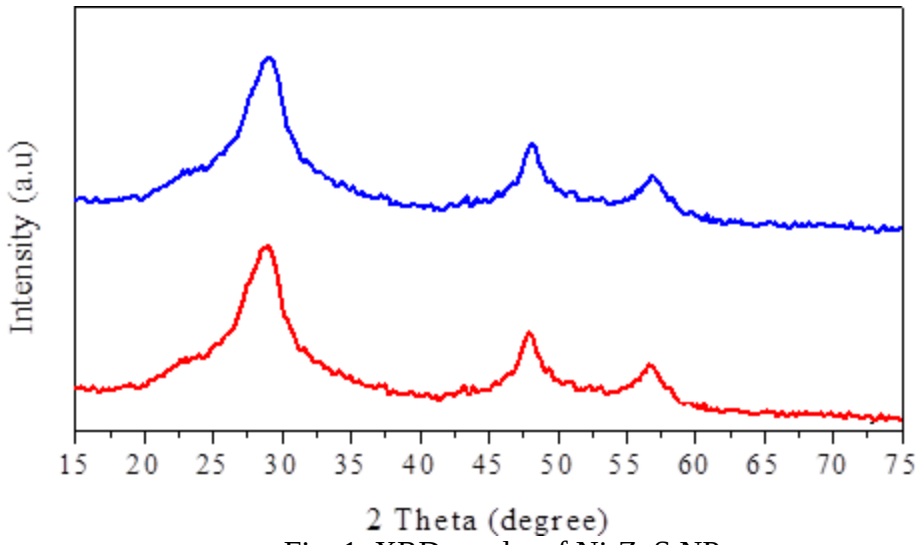

Fig. 1. XRD results of Ni-ZnS NPs

FT-IR analysis

FT-IR spectrum of pure phase Ni-ZnS is shown in Fig. 2. FT-IR spectra exhibit a common broad band near 3425 cm^{-1} and 1625 cm is due to the stretching and bending vibrations of hydrogen-bonded –OH groups [28]. The band at around 1380 cm^{-1} has been assigned to stretching modes of -N-H group. It was found that two strong absorption band at lower frequency can be assigned to the M-S (M = Ni and Zn) bonds [29, 30].

e-ISSN 2320 –7876 www.ijfans.org
Vol.11, Iss.9, Dec 2022

Research Paper

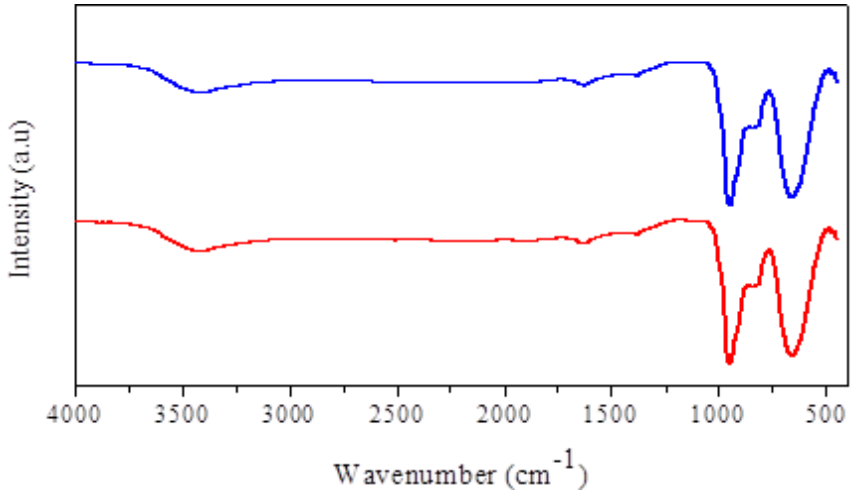

Fig. 2. FT-IR results of Ni-ZnS NPs

HR-SEM analysis

Fig. 3 shows the SEM images of Ni-ZnS. From the SEM images, crystallites agglomerate and form particles and rods with diameters of below 60 nm for a synthesis time of 10 min, and there is a greater variation in size with Ni-doping. We believe that this aggregation process is related to the increase in effective collision rates between small particles by microwave irradiation.

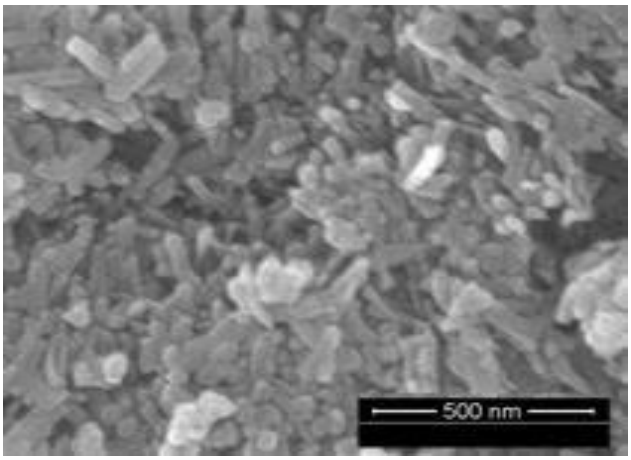

Fig. 3. SEM images of Ni-ZnS NPs

TEM analysis

Fig. 4 shows the HR-TEM images of Ni-ZnS, consist of many nanorods structure and irregular shaped nano-particles are jointed together. Fig. 4 displays the SAED pattern of the

samples. The rings are diffuse and hollow showing that the products are composed of very fine particles with highly crystalline in nature.

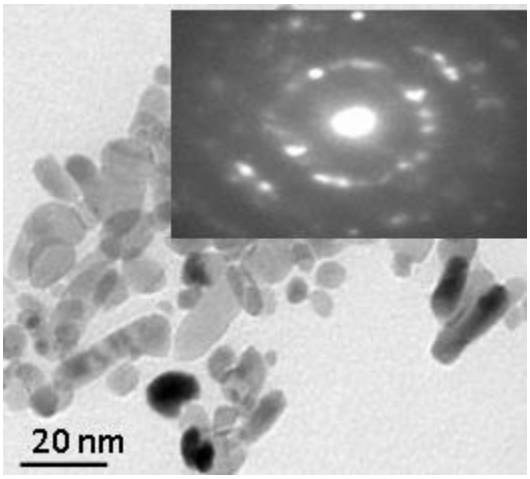

Fig. 4. TEM images of Ni-ZnS NPs

EDX analysis

The chemical composition of Ni-ZnS NPs was analyzed by energy dispersive X-ray analysis (EDX). The results show that the as-prepared Ni-ZnS NPs are elementally pure and there is no other peak is formed. However, a small peak appeared at 2.1 KeV for undoped and Ni-ZnS NPs, which indicates the presence of Au peak that has been used as a sputter coating, while preparing the sample for SEM analysis for the better visibility of the surface morphology.

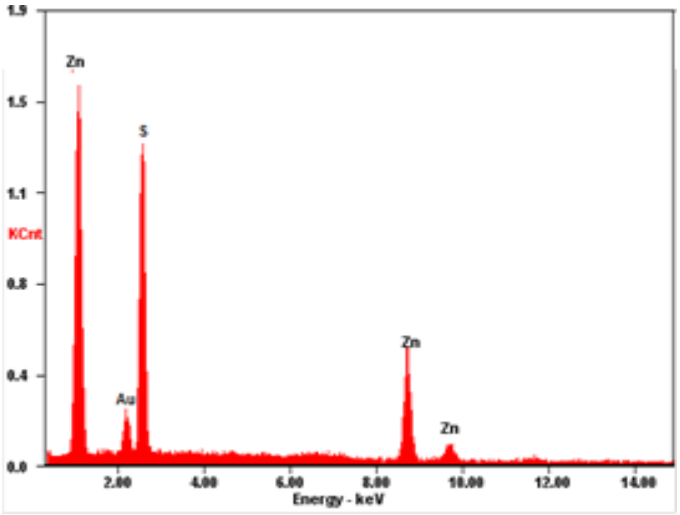

Fig. 5. EDX spectra of Ni-ZnS NPs

e-ISSN 2320 –7876 www.ijfans.org
Vol.11, Iss.9, Dec 2022

Research Paper

UV-Visible DRS analysis

The band gap energy (E_g) of the obtained Ni-ZnS NPs was determined from the UV-Vis DRS spectra recorded at room temperature. The value of E_g was calculated using Tauc relation. The Kubelka-Munk function is generally applied to convert the DRS into equivalent absorption coefficient and mostly used for analyzing the powder samples. The E_g of nano-crystals can be calculated using the Kubelka-Munk model and the F(R) value is estimated. Thus the vertical axis is converted into quantity $F(R)$ which is equal to the absorption co-efficient. Thus the *'α'* in the Tauc equation is substituted with $F(R)$ and hence the relation becomes,

$$(F(R)) = \alpha = \frac{(1-R)^2}{2R} \qquad \text{---- (3)}$$

where, F(R) is Kubelka-Munk function, *'α'* the absorption coefficient, *'R'* the reflectance. Thus the Tauc relation becomes,

$$F(R)h\upsilon = A(h\upsilon - E_g)^n \text{----------} \quad (4)$$

where n = 1/2 and 2 for direct and indirect transitions, respectively, thus giving direct and indirect band gaps. The plots of $(F(R)h\upsilon)^2$ versus hυ for all compositions are shown in Fig. 5. Extrapolation of linear regions of these plots to $(F(R)h\upsilon)^2 = 0$ gives the direct band gap values. The exponential optical absorption edge and the E_g values are controlled by the degree of structural disorder in the lattice.

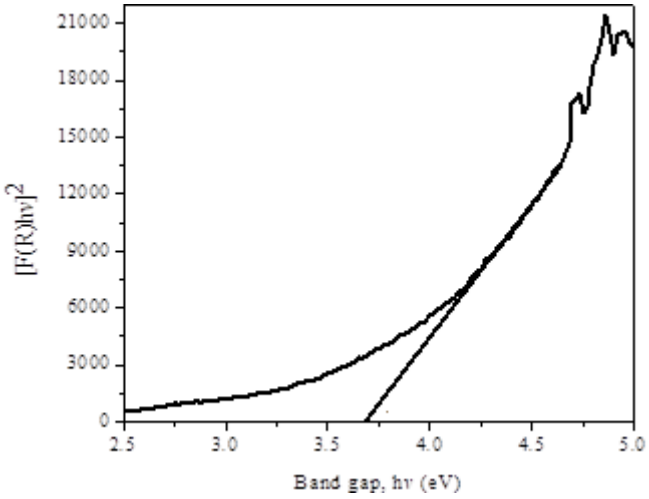

Fig. 6. UV-Vis DRS spectra of Ni-ZnS NPs

e-ISSN 2320 –7876 www.ijfans.org
Vol.11, Iss.9, Dec 2022

Research Paper

Photoluminescence (PL) studies

Fig. 7 shows PL evolutions of Ni-ZnS NPs. It is well known that due to their very small diameter of the nano-crystals has a very high ratio of surface to volume that makes them susceptible to various surface defects. In most reported works the sources of PL are attributed to self-activated centers and these centers in turn to crystal lattice vacancies such as sulfur vacancies [25]. As a result, it appears that microwave heating treatment could be an effective tool to control the physico-chemical properties of metal sulfide nano-crystallites such as crystal phase, size, morphology, and luminescence, when combined with proper heating treatment and time.

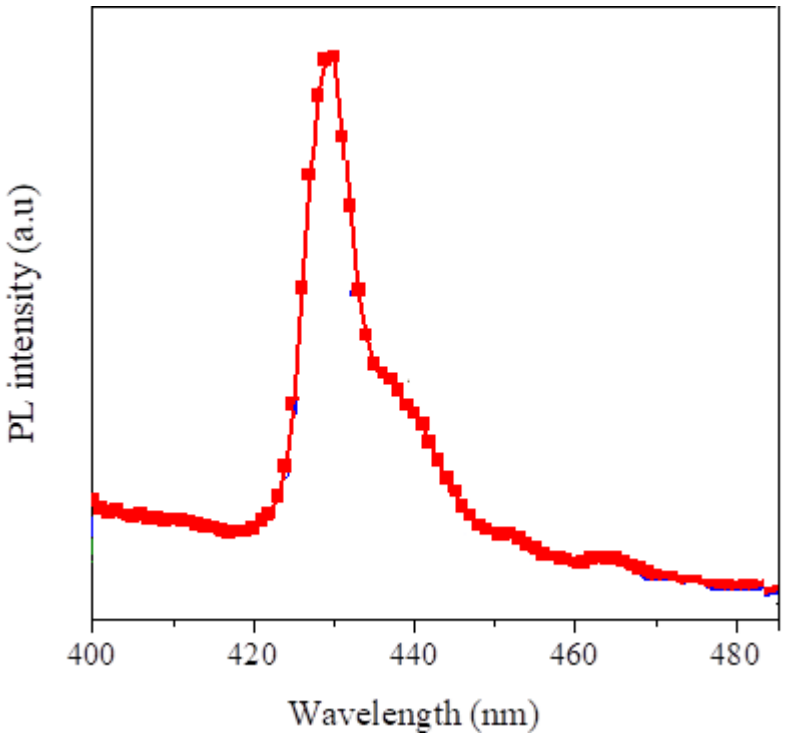

Fig. 7. PL spectra of Ni-ZnS NPs

3.8 VSM analysis

Fig. 8 shows the VSM measurements of Ni-ZnS NPs. The shapes of magnetic hysteresis, *M-H* curves indicate that ferromagnetic for Ni-ZnS NPs. The observation of ferromagnetic behavior indicates that the Ni^{2+} ions have been substituted the Zn^{2+} sites without changing the cubic structure of ZnS. The *M-H* curves show that the saturation magnetization (M_s) values are increased with increasing the Ni-doping at room temperature. The increase in the values of M_s by

increasing the Mn content can be attributed to the higher magnetic moment of Mn^{2+}. Since the higher magnetic moment of Ni^{2+} ions (3 μ_B) replace the non-magnetic nature of Zn^{2+} ions (0 μ_B) by increasing the composition, and hence the values of M_s is found to increased. However, M_s, M_r and H_c values are depend on the particle size, crystallinity, nature and composition of the dopant. The magnetic properties of semiconductor nanomaterials are highly dependent on the crystal structure, surface morphology, geometry, nature and concentration of the doping metal cations, anisotropy, etc.

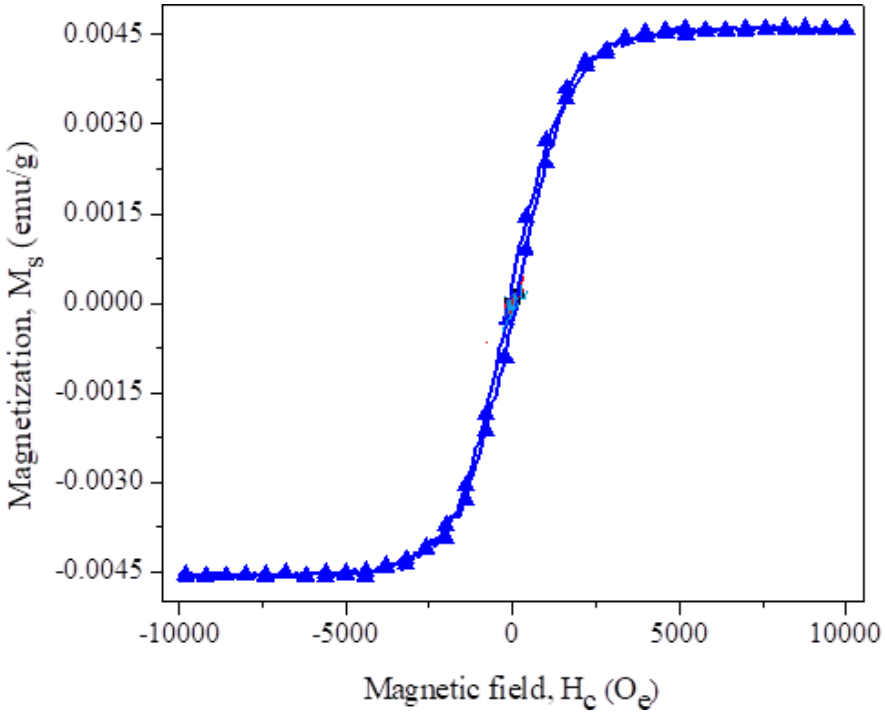

Fig. 8. VSM results of Ni-ZnS NPs

4. Conclusions

Single phase Ni-ZnS NPs have been successfully synthesized by a facile, one-pot microwave combustion route. Powder XRD, FT-IR, EDX and SAED results confirmed the formation of single phase Ni-ZnS NPs. It was found that the average crystallite size and morphology of Ni-ZnS NPs are dependent on the microwave heating treatment and metal doping concentration. The formation of irregular shaped aggregated rods with spherical shaped particle-like nano-crystals was confirmed by HR-SEM and HR-TEM analysis. The E_g of undoped ZnS is

3.60 eV and it is increased from 3.65 eV to 3.67 eV with increasing the Mn^{2+} ions (x = 0.3-0.5), and the as-prepared samples showed good opto-magnetic and catalytic properties. M-H loop of the as-synthesized Ni-ZnS NPs showed weak ferromagnetic behavior. The M_s values increased with increasing the concentration of Mn^{2+} ions. It is interesting to note that the microwave heating is able to reduce time of the reactions, and can rapidly yielded such functional nano-crystals.

References

[1]. O. Alagha, N. Ouerfelli, H. Kochkar, M. A. Almessiere , Y. Slimani, A. Manikandan, A. Baykal, A. Mostafa, M. Zubair, M. H. Barghouthi, Kinetic Modeling for Photo-Assisted Penicillin G Degradation of $(Mn_{0.5}Zn_{0.5})[Cd_xFe_{2-x}]O_4$ ($x \leq 0.05$) Nanospinel Ferrites, Nanomaterials, 11 (2021) 970.

[2]. M. R. Ranjitha, A. Manikandan, J. N. Baby, K. Panneerselvam, S. Ragu, Mary George, Y. Slimani, M.A. Almessiere, A. Baykal, Hexagonal basalt-like ceramics $La_xMg_{1-x}TiO_3$ (x = 0 and 0.5) contrived via deep eutectic solvent for selective electrochemical detection of dopamine, Physica B: Condensed Matter, 615 (2021) 413068.

[3]. M. A. Almessiere, B. Unal, I.A. Auwal, Y. Slimani, H. Aydin, A. Manikandan, A. Baykal, Impact of calcination temperature on electrical and dielectric properties of $SrGa_{0.05}Fe_{11.98}O_4$-$Zn_{0.5}Ni_{0.5}Fe_2O_4$ hard/soft nanocomposites, Journal of Materials Science: Materials in Electronics, 32 (2021) 16589-16600.

[4]. S. S. Al-Jameel, M. A. Almessiere, F. A. Khan, N. Taskhandi , Y. Slimani, N. S. Al-Saleh, A. Manikandan, E. A. Al-Suhaimi, A. Baykal, Synthesis, Characterization, Anti-Cancer Analysis of $Sr_{0.5}Ba_{0.5}Dy_xSm_xFe_{8-2x}O_{19}$ ($0.00 \leq x \leq 1.0$) Microsphere Nanocomposites, Nanomaterials, 11 (2021) 700.

[5]. M. A. Almessiere, Y. Slimani, H. Güngüneş, K. A. Demir, Z. Tatiana, T. Sergei, T. Alex, A. Manikandan, A. Fatimah, A. Baykal, Influence of Dy^{3+} ions on microstructure, magnetic, electrical and microwave properties of $[Ni_{0.4}Cu_{0.2}Zn_{0.4}](Fe_{2-x}Dy_x)O_4$ ($0.00<x<0.04$) spinel ferrites, ACS Omega, 6 (2021) 10266-10280.

[6]. P. Annie Vinosha, A. Manikandan, A. Christy Preetha, A. Dinesh, Y. Slimani, M.A. Almessiere, A. Baykal, Belina Xavier, G. Francisco Nirmala, Review on recent

advances of synthesis, magnetic properties and water treatment applications of cobalt ferrite nanoparticles and nanocomposites, Journal of Superconductivity and Novel Magnetism, 34 (2021) 995–1018.

[7]. K. Elayakumar, A. Manikandan, A. Dinesh, K. Thanrasu, K. Kanmani Raja, R. Thilak Kumar, Y. Slimani, S. K. Jaganathan, A. Baykal, Enhanced magnetic property and antibacterial biomedical activity of Ce^{3+} doped $CuFe_2O_4$ spinel nanoparticles synthesized by sol-gel method, J. Magn. Magn. Mater. 478 (2019) 140–147.

[8]. A. Godlyn Abraham, A. Manikandan, E. Manikandan, S. Vadivel, S. K. Jaganathan, A. Baykal, P. Sri Renganathan, Enhanced magneto-optical and photo-catalytic properties of transition metal cobalt (Co^{2+} ions) doped spinel $MgFe_2O_4$ ferrite nanocomposites, J. Magn. Magn. Mater. 452 (2018) 380-388.

[9]. M. Maria Lumina Sonia, S. Anand, S. Blessi, S. Pauline, A. Manikandan, Effect of surfactants (PVB/EDTA/CTAB) assisted sol-gel synthesis on structural, magnetic and dielectric properties of $NiFe_2O_4$ nanoparticles, Ceram. Int. 44 (2018) 22068-22079.

[10]. K. Elayakumar, A. Dinesh, A. Manikandan, P. Murugesan, G. Kavitha, S. Prakash, R. Thilak Kumar, S. K. Jaganathan, A. Baykal, Structural, morphological, enhanced magnetic properties and antibacterial bio-medical activity of rare earth element (REE) Cerium (Ce^{3+}) doped $CoFe_2O_4$ nanoparticles, J. Magn. Magn. Mater. 476 (2019) 157-165.

[11]. Md Amir, H. Gungunes, A. Baykal, M. Almessiere, H. Sozeri, I. Ercan, M. Sertkol, S. Asiri, A Manikandan, Effect of annealing temperature on Magnetic and Mossbauer properties of $ZnFe_2O_4$ nanoparticles by sol-gel approach, J. Supercond. Nov. Magn. 31 (2018) 3347–3356.

[12]. I. J. C. Lynda, M. Durka, A. Dinesh, A. Manikandan, S. K. Jaganathan, A. Baykal, S. Arul Antony, Enhanced Magneto-optical and Photocatalytic Properties of Ferromagnetic $Mg_{1-y}Ni_yFe_2O_4$ ($0.0 \leq y \leq 1.0$) Spinel Nano-ferrites, J. Supercond. Nov. Magn. 31 (2018) 3637–3647.

[13]. M. Maria Lumina Sonia, S. Anand, V. Maria Vinosel, M. Asisi Janifer, S. Pauline, A. Manikandan, Effect of lattice strain on structure, morphology and magneto-dielectric properties of $NiGd_xFe_{2-x}O_4$ ferrite nano-crystallites synthesized by sol-gel route, J. Magn. Magn. Mater. 466 (2018) 238-251.

[14]. A. Godlyn Abraham, A. Manikandan, E. Manikandan, S. K. Jaganathan, A. Baykal, P. Sri Renganathan, Enhanced Opto-Magneto Properties of $Ni_xMg_{1-x}Fe_2O_4$ ($0.0 \leq x \leq 1.0$) Ferrites Nano-Catalysts, J. Nanoelect. Optoelect. 12 (2017) 1326–1333

[15]. S. Asiri, M. Sertkol, S. Guner, H. Gungunes, K.M. Batoo, T.A. Saleh, H. Sozeri, M.A. Almessiere, A. Manikandan, A. Baykal, Hydrothermal synthesis of $Co_yZn_yMn_{1-2y}Fe_2O_4$ nanoferrites: Magneto-optical investigation, Ceram. Int. 44 (2018) 5751–5759.

[16]. A. Baykal, S. Guner, H. Gungunes, K.M. Batoo, Md. Amir, A. Manikandan, Magneto Optical Properties and hyperfine interactions of Cr^{3+} ion substituted copper ferrite nanoparticles, J. Inorg. Organomet. Polym. 28 (2018) 2533–2544,

[17]. E. Hema, A. Manikandan, P. Karthika, M. Durka, S. Arul Antony, B. R. Venkatraman, Magneto-optical properties of recyclable spinel $Ni_xMg_{1-x}Fe_2O_4$ ($0.0 \leq x \leq 1.0$) nano-catalysts, J. Nanosci. Nanotech. 16 (2016) 7325-7336.

[18]. Y. Slimani, A. Baykal, Md. Amir, N. Tashkandi, H. Güngüneş, S. Guner, H.S. El Sayed, F. Aldakheel, T.A. Saleh, A. Manikandan, Substitution effect of Cr^{3+} on hyperfine interactions, magnetic and optical properties of Sr-hexaferrites, Ceram. Int. 44 (2018) 15995-16004.

[19]. Y. Slimani, H. Gungunes, M. Nawaz, A. Manikandan, H.S. El Sayed, M.A. Almessiere, H. Sozeri, S.E. Shirsath, I. Ercan, A. Baykal, Magneto-optical and microstructural properties of spinel cubic copper ferrites with Li-Al co-substitution, Ceram. Int. 44 (2018) 14242-14250.

[20]. S. Asiri, S. Güner, A. Demir, A. Yildiz, A. Manikandan, A. Baykal, Synthesis and Magnetic Characterization of Cu Substituted Barium Hexaferrites, J. Inorg. Organomet. Polym. Mater. 28 (2018) 1065–1071.

[21]. A. Silambarasu, A. Manikandan, K. Balakrishnan, Room temperature superparamagnetism and enhanced photocatalytic activity of magnetically reusable spinel $ZnFe_2O_4$ nano-catalysts, J. Supercond. Nov. Magn. 30 (2017) 2631–2640.

[22]. G. Padmapriya, A. Manikandan, V. Krishnasamy, S. K. Jaganathan, S. Arul Antony, Enhanced catalytic activity and magnetic properties of spinel $Mn_xZn_{1-x}Fe_2O_4$ ($0.0 \leq x \leq 1.0$) nano-photocatalysts by microwave irradiation route, J. Supercond. Nov. Magn. 29 (2016) 2141-2149.

[23]. S. Gunasekaran, K. Thanrasu, A. Manikandan, M. Durka, A. Dinesh, S. Anand, S. Shankar, Y.Slimani, M. A. Almessiere, A. Baykal, Structural, fabrication and enhanced electromagnetic wave absorption properties of reduced graphene oxide (rGO)/zirconium substituted cobalt ferrite ($Co_{0·5}Zr_{0·5}Fe_2O_4$) nanocomposites, Physica B: Condensed Matter, 605 (2021) 412784.

[24]. F. Hussain, S. Z. Shah, H. Ahmad, S. A. Abubshait, H. A. Abubshait, A. Laref, A. Manikandan, H. S. Kusuma, M. Iqbal, Microalgae an ecofriendly and sustainable wastewater treatment option: Biomass application in biofuel and bio-fertilizer production. A review, Renewable and Sustainable Energy Reviews, 137 (2021) 110603.

[25]. P. A. Vinosha, A. Manikandan, A. S. J. Ceicilia, A. Dinesh, G. F. Nirmala, A. Christy Preetha, Y. Slimani, M.A. Almessiere, A. Baykal, B. Xavier, Review on recent advances of zinc substituted cobalt ferrite nanoparticles: Synthesis characterization and diverse applications, Ceramics International, 47 (2021) 10512-10535.

[26]. S. Blessi, S. Anand, A. Manikandan, M. M. Lumina Sonia, V. Maria Vinosel, Y. Slimani, M.A. Almessiere, A. Baykal, Structural, optical and electrochemical investigations of Sb substituted mesoporous SnO_2 nanoparticles, Journal of Materials Science: Materials in Electronics, 32 (2021) 4132–4145.

[27]. Y. Slimani, N. A. Algarou, M. A. Almessiere, A. Sadaqat M. G. Vakhitov, D. S. Klygach, D. I. Tishkevich, A. V. Trukhanov, S. Güner, A. S. Hakeem, I. A. Auwal, A. Baykal, A. Manikandan, I. Ercan, Fabrication of exchanged coupled hard/soft magnetic nanocomposites: Correlation between composition, magnetic, optical and microwave properties, Arabian Journal of Chemistry, 10 (2021) 102992.

[28]. P. Manimaran, S. Balasubramaniyan, M. Azam, D. Rajadurai, S. I. Al-Resayes, G. Mathubala, A. Manikandan, S. Muthupandi, Z. Tabassum, I. Khan, Synthesis, Spectral Characterization and Biological Activities of Co(II) and Ni(II) Mixed Ligand Complexes, Molecules, 26 (2021) 823.

[29]. K. Geetha, R. Udhayakumar, A. Manikandan, Enhanced magnetic and photocatalytic characteristics of cerium substituted spinel $MgFe_2O_4$ ferrite nanoparticles, Physica B: Physics of Condensed Matter, 615 (2021) 413083.

[30]. S. S. Al-Jameel, S. Rehman, M. A. Almessiere, F. A. Khan, Y. Slimani, N. S. Al-Saleh, A. Manikandan, E. A. Al-Suhaimi, A. Baykal, Anti-microbial and anti-cancer activities of $MnZnDy_xFe_{2-x}O_4$ ($x \leq 0.1$) nanoparticles, Artificial Cells, Nanomedicine and Biotechnology, 49 (2021) 493-499.

[31]. S. Rehman, M. A. Almessiere, S. S. Al-Jameel, U. Ali, Y. Slimani, N. Taskhandi, N. S. Al-Saleh, A. Manikandan, F. A. Khan, E. A. Al-Suhaimi, A. Baykal, Designing of $Co_{0.5}Ni_{0.5}Ga_xFe_{2-x}O_4$ ($0.0 \leq x \leq 1.0$) Microspheres via Hydrothermal Approach and Their Selective Inhibition on the Growth of Cancerous and Fungal Cells, Pharmaceutics, 13 (2021) 962.

[32]. M. A. Almessiere, B. Unal, Y. Slimani, H. Gungunes, M. S. Toprak, N. Tashkand, A. Baykal, M. Sertkol, A.V. Trukhanov, A. Yıldız, A. Manikandan, Effects of Ce-Dy rare earths co-doping on various features of Ni-Co spinel ferrite microspheres prepared via hydrothermal approach, J. of Materials Research and Technology, 14 (2021) 2534-2553.

[33]. S. Blessi, A. Manikandan, S. Anand, M. M. L. Sonia, V. M. Vinosel, P. Paulraj, Y. Slimani, M.A. Almessiere, M. Iqbal, S. Guner, A. Baykal, Effect of Zinc substitution on the physical and electrochemical properties of mesoporous SnO_2 nanomaterials, Materials Chemistry and Physics, 273 (2021) 125122.

[34]. M. A. Almessiere, Y. Slimani, Y. O. Ibrahim, M. A. Gondal, M. A. Dastageer, I. A. Auwal, A. V. Trukhanov, A. Manikandan, A. Baykal, Morphological, structural, and magnetic characterizations of hard-soft ferrite nanocomposites synthesized via pulsed laser ablation in liquid, Materials Science and Engineering B, 273 (2021) 115446.

[35]. S. Blessi, S. Anand, A. Manikandan, M. Maria Lumina Sonia, V. Maria Vinosel, Y. Slimani, M.A. Almessiere, A. Baykal, Influence of Ni substitution on opto-magnetic and electrochemical properties of CTAB capped mesoporous SnO_2 nanoparticles, Journal of Materials Science: Materials in Electronics, Journal of Materials Science: Materials in Electronics, 32 (2021) 7630–7646.

[36]. M. George, T.L. Ajeesha, A. Manikandan, Ashwini Anantharaman, R.S. Jansi, E. Ranjith Kumar, Y. Slimani, M.A. Almessiere, A. Baykal, Evaluation of Cu-$MgFe_2O_4$ spinel nanoparticles for photocatalytic and antimicrobial activates, Journal of Physics and Chemistry of Solids, 153 (2021) 110010.